CURFIL: Random Forests for Image Labeling on GPU

Hannes Schulz, Benedikt Waldvogel, Rasha Sheikh and Sven Behnke
University of Bonn, Computer Science Institute VI, Autonomous Intelligent Systems,
Friedrich-Ebert-Allee 144, 53113 Bonn, Germany

Keywords: Random Forest, Computer Vision, Image Labeling, GPU, CUDA.

Abstract: Random forests are popular classifiers for computer vision tasks such as image labeling or object detection. Learning random forests on large datasets, however, is computationally demanding. Slow learning impedes model selection and scientific research on image features. We present an open-source implementation that significantly accelerates both random forest learning and prediction for image labeling of RGB-D and RGB images on GPU when compared to an optimized multi-core CPU implementation. We use the fast training to conduct hyper-parameter searches, which significantly improves on previous results on the NYU depth v2 dataset. Our prediction runs in real time at VGA resolution on a mobile GPU and has been used as data term in multiple applications.

1 INTRODUCTION

Random forests are ensemble classifiers that are popular in the computer vision community. Random decision trees are used when the hypothesis space at every node is huge, so that only a random subset can be explored during learning. This restriction is countered by constructing an ensemble of independently learned trees—the random forest.

Variants of random forests were used in computer vision to improve e.g. object detection or image segmentation. One of the most prominent examples is the work of (Shotton et al., 2011), who use random forests in Microsoft's Kinect system for the estimation of human pose from single depth images. Here, we are interested in the more general task of image labeling, i.e. determining a label for every pixel in an RGB or RGB-D image (Fig. 1).

The real-time applications such as the ones presented by (Lepetit et al., 2005) and (Shotton et al., 2011) require fast prediction in few milliseconds per image. This is possible with parallel architectures such as GPUs, since every pixel can be processed independently. Random forest training for image labeling, however, is not as regular—it is a time consuming process. To evaluate a randomly generated feature candidate in a single node of a single tree, a potentially large number of images must be accessed. With increasing depth, the number of pixels in an image arriving in the current node can be very small. It is therefore essential for the practitioner to optimize memory efficiency in various regimes, or to resort to large clusters for the computation. Furthermore, changing the visual features and other hyper-parameters requires a re-training of the random forest, which is costly and impedes efficient scientific research.

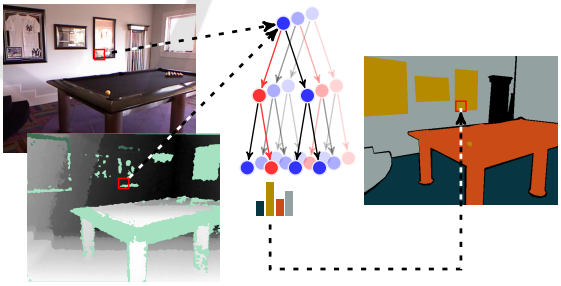

Figure 1: Overview of image labeling with random forests: Every pixel (RGB and depth) is classified independently based on its context by the trees of a random forest. The leaf distributions of the trees determine the predicted label.

This work describes the architecture of our open-source GPU implementation of random forests for image labeling (CURFIL). CURFIL provides optimized CPU and GPU implementations for the training and prediction of random forests. Our library trains random forests up to 26 times faster on GPU than our optimized multi-core CPU implementation. Prediction is possible in real-time speed on a single mobile GPU.

In short, our contributions are as follows:

1. we describe how to efficiently implement random forests for image labeling on GPU,
2. we describe a method which allows to train on

Schulz H., Waldvogel B., Sheikh R. and Behnke S..
CURFIL: Random Forests for Image Labeling on GPU.
DOI: 10.5220/0005316201560164
In *Proceedings of the 10th International Conference on Computer Vision Theory and Applications* (VISAPP-2015), pages 156-164
ISBN: 978-989-758-090-1

horizontally flipped images at significantly reduced cost,
3. we show that our GPU implementation is up to 26 times faster for training (up to 48 times for prediction) than an optimized multi-core CPU implementation,
4. we show that simply by the now feasible optimization of hyper-parameters, we can improve performance in two image labeling tasks, and
5. we make our documented, unit-tested, and MIT-licensed source code publicly available[1].

The remainder of this paper is organized as follows. After discussing related work, we introduce random forests and our node tests in Sections 3 and 4, respectively. We describe our optimizations in Section 5. Section 6 analyzes speed and accuracy attained with our implementation.

2 RELATED WORK

Random forests were popularized in computer vision by (Lepetit et al., 2005). Their task was to classify patches at pre-selected keypoint locations, not—as in this work—all pixels in an image. Random forests proved to be very efficient predictors, while training efficiency was not discussed. Later work focused on improving the technique and applying it to novel tasks.

(Lepetit and Fua, 2006) use random forests to classify keypoints for object detection and pose estimation. They evaluate various node tests and show that while training is increasingly costly, prediction can be very fast.

The first GPU implementation for our task was presented by (Sharp, 2008), who implements random forest training and prediction for Microsoft's Kinect system that achieves a prediction speed-up of 100 and training speed-up factor of eight on a GPU, compared to a CPU. This implementation is not publicly available and uses Direct3D which is only supported on the Microsoft Windows platform.

An important real-world application of image labeling with random forests is presented by (Shotton et al., 2011). Human pose estimation is formulated as a problem of determining pixel labels corresponding to body parts. The authors use a distributed CPU implementation to reduce the training time, which is nevertheless one day for training three trees from one million synthetic images on a 1,000 CPU core cluster. Their implementation is also not publicly available.

Several fast implementations for general-purpose random forests are available, notably in the *scikit-learn* machine learning library (**?**) for CPU and *CudaTree* (Liao et al., 2013) for GPU. General random forests cannot make use of texture caches optimized for images though, i.e., they treat all samples separately. GPU implementations of general-purpose random forests also exist, but due to the irregular access patterns when compared to image labeling problems, their solutions were found to be inferior to CPU (Slat and Lapajne, 2010) or focused on prediction (Van Essen et al., 2012).

The prediction speed and accuracy of random forests facilitates applications interfacing computer vision with robotics, such as semantic prediction in combination with self localization and mapping (Stückler et al., 2012) or 6D pose estimation (Rodrigues et al., 2012) for bin picking.

CURFIL was successfully used by (Stückler et al., 2013) to predict and accumulate semantic classes of indoor sequences in real-time, and by (Müller and Behnke, 2014) to significantly improve image labeling accuracy on a benchmark dataset.

3 RANDOM FORESTS

Random forests—also known as random decision trees or random decision forests—were independently introduced by (Ho, 1995) and (Amit and Geman, 1997). (Breiman, 2001) coined the term "random forest". Random decision forests are ensemble classifiers that consist of multiple decision trees—simple, commonly used models in data mining and machine learning. A decision tree consists of a hierarchy of questions that are used to map a multi-dimensional input value to an output which can be either a real value (regression) or a class label (classification). Our implementation focuses on classification but can be extended to support regression.

To classify input x, we traverse each of the K decision trees $\mathcal{T}_k$ of the random forest $\mathcal{F}$, starting at the root node. Each inner node defines a test with a binary outcome (i.e. true or false). We traverse to the left child if the test is positive and continue with the right child otherwise. Classification is finished when a leaf node $l_k(x)$ is reached, where either a single class label or a distribution $p(c \mid l_k(x))$ over class labels $c \in \mathcal{C}$ is stored.

The K decision trees in a random forest are trained independently. The class distributions for the input x are collected from all leaves reached in the decision trees and combined to generate a single classification. Various combination functions are possible. We implement majority voting and the average of all probability

[1] https://github.com/deeplearningais/curfil/

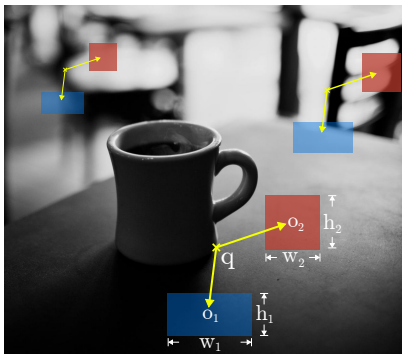

Figure 2: Sample visual feature at three different query pixels. Feature response is calculated from difference of average values in two offset regions. Relative offset locations $\mathbf{o}_i$ and region extents w_i, h_i are normalized with the depth $d(\mathbf{q})$ at the query pixel $\mathbf{q}$.

distributions as defined by

$$p(c\,|\,\mathcal{F},x) = \frac{1}{K}\sum_{k=1}^{K} p(c\,|\,l_k(x)).$$

Key difference between a decision tree and a random decision tree is the training phase. The idea of random forests is to train multiple trees on different random subsets of the dataset and random subsets of features. In contrast to normal decision trees, random decision trees are not pruned after training, as they are less likely to overfit (Breiman, 2001). Breiman's random forests use CART as tree growing algorithm and are restricted to binary trees for simplicity. The best split criterion in a decision node is selected according to a score function measuring the separation of training examples. CURFIL supports information gain and normalized information gain (Wehenkel and Pavella, 1991) as score functions.

A special case of random forests are random ferns, which use the same feature in all nodes of a hierarchy level. While our library also supports ferns, we do not discuss them further in this paper, as they are neither faster to train nor did they produce superior results.

4 VISUAL FEATURES FOR NODE TESTS

Our selection of features was inspired by (Lepetit et al., 2005)—the method for visual object detection proposed by (Viola and Jones, 2001). We implement two types of RGB-D image features as introduced by (Stückler et al., 2012). They resemble the features of (Sharp, 2008; Shotton et al., 2011)—but use depth-normalization and region averages instead of single pixel values. (Shotton et al., 2011) avoid the use of region averages to keep computational complexity low. For RGB-only datasets, we employ the same features but assume constant depth. The features are visualized in Fig. 2.

Algorithm 1: Training of random decision tree.

Require: $\mathcal{D}$ training instances
Require: F number of feature candidates to generate
Require: P number of feature parameters
Require: T number of thresholds to generate
Require: stopping criterion (e.g. maximal depth)

$D \leftarrow$ randomly sampled subset of $\mathcal{D}$ ($D \subset \mathcal{D}$)
$N_{\text{root}} \leftarrow$ create root node
$C \leftarrow \{(N_{\text{root}}, D)\}$ ▷ initialize candidate nodes
while $C \neq \emptyset$ **do**
  $C' \leftarrow \emptyset$ ▷ initialize new set of candidate nodes
  for all $(N, D) \in C$ **do**
    $(D_{\text{left}}, D_{\text{right}}) \leftarrow$ EVALBESTSPLIT(D)
    if $\neg$STOP(N, D_{left}) **then**
      $N_{\text{left}} \leftarrow$ create left child for node N
      $C' \leftarrow C' \cup \{(N_{\text{left}}, D_{\text{left}})\}$
    if $\neg$STOP(N, D_{right}) **then**
      $N_{\text{right}} \leftarrow$ create right child for node N
      $C' \leftarrow C' \cup \{(N_{\text{right}}, D_{\text{right}})\}$
  $C \leftarrow C'$ ▷ continue with new set of nodes

For a given query pixel $\mathbf{q}$, the image feature f_θ is calculated as the difference of the average value of the image channel ϕ_i in two rectangular regions R_1, R_2 in the neighborhood of $\mathbf{q}$. Size w_i, h_i and 2D offset $\mathbf{o}_i$ of the regions are normalized by the depth $d(\mathbf{q})$:

$$f_\theta(\mathbf{q}) := \frac{1}{|R_1(\mathbf{q})|}\sum_{\mathbf{p}\in R_1}\phi_1(\mathbf{p}) - \frac{1}{|R_2(\mathbf{q})|}\sum_{\mathbf{p}\in R_2}\phi_2(\mathbf{p})$$

$$R_i(\mathbf{q}) := \left(\mathbf{q} + \frac{\mathbf{o}_i}{d(\mathbf{q})}, \frac{w_i}{d(\mathbf{q})}, \frac{h_i}{d(\mathbf{q})}\right). \quad (1)$$

CURFIL optionally fills in missing depth measurements. We use integral images to efficiently compute region sums. The large space of eleven feature parameters—region sizes, offsets, channels, and thresholds—requires to calculate feature responses on-the-fly since pre-computing all possible values in advance is not feasible.

5 CURFIL SOFTWARE PACKAGE

CURFIL's speed is the result of careful optimization of GPU memory throughput. This is a non-linear process to find fast combinations of memory layouts, algorithms and exploitable hardware capabilities. In the following, we describe the most relevant aspects of our implementation.

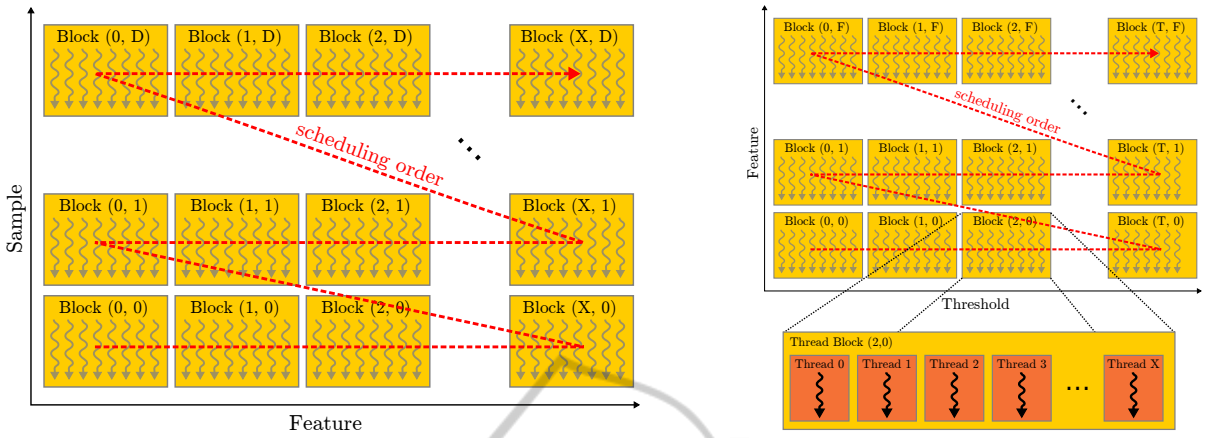

(a) Feature Response Kernel (b) Histogram Aggegation Kernel

Figure 3: **(a)** Two-dimensional grid layout of the feature response kernel for D samples and F features. Each block contains n threads. The number of blocks in a row, X, depends on the number of features. $X = \lceil F/n \rceil$. Feature responses for a given sample are calculated by the threads in one block row. The arrow (red dashes) indicates the scheduling order of blocks. **(b)** Thread block layout of the histogram aggregation kernel for F features and T thresholds. One thread block per feature and per threshold. X threads in block aggregate histogram counters for D samples in parallel. Every thread iterates over at most $\lceil D/X \rceil$ samples.

User API. The CURFIL software package includes command line tools as well as a library for random forest training and prediction. Inputs consist of images for RGB, depth, and label information. Outputs are forests in JSON format for training and label-images for prediction. Datasets with varying aspect ratios are supported.

Our source code is organized such that it is easy to improve and change the existing visual feature implementation. It is developed in a test-driven process. Unit tests cover major parts of our implementation.

CPU Implementation. Our CPU implementation is based on a refactored, parallelized and heavily optimized version of the *Tuwo Computer Vision Library*[2] by Nowozin. Our optimizations make better use of CPU cache by looping over feature candidates and thresholds in the innermost loop, and by sorting the dataset according to image before learning. Since feature candidate evaluations do not depend on each other, we can parallelize over the training set and make use of all CPU cores even when training only a single tree.

GPU Implementation. Evaluation of the optimized random forest training on CPU (Algorithm 1) shows that the vast majority of time is spent in the evaluation of the best split feature. This is to our benefit when accelerating random forest training on GPU. We restrict the GPU implementation efforts to the relatively short feature evaluation algorithm (Algorithm 2) as a drop-in replacement and leave the rest of the CPU computation unchanged. We use the CPU implementation as a reference for the GPU and ensure that results are the same in both implementations.

Split evaluation can be divided into the following four phases that are executed in sequential order:

1. random feature and threshold candidate generation,
2. feature response calculation,
3. histogram aggregation for all features and threshold candidates, and
4. impurity score (information gain) calculation.

Each phase depends on results of the previous phase. As a consequence, we cannot execute two or more phases in parallel. The CPU can prepare data for the launch of the next phase, though, while the GPU is busy executing the current phase.

Algorithm 2: CPU-optimized feature evaluation.

Require: D samples
Require: $\mathbf{F} \in \mathbb{R}^{F \times P}$ random feature candidates
Require: $\mathbf{T} \in \mathbb{R}^{F \times T}$ random threshold candidates
initialize histograms for every feature/threshold
for all $d \in D$ **do**
  for all $f \in 1 \ldots F$ **do**
    calculate feature response
    for all $\theta \in \mathbf{T}_f$ **do**
      update according histogram
calculate impurity scores for all histograms
return histogram with best score

[2] http://www.nowozin.net/sebastian/tuwo/

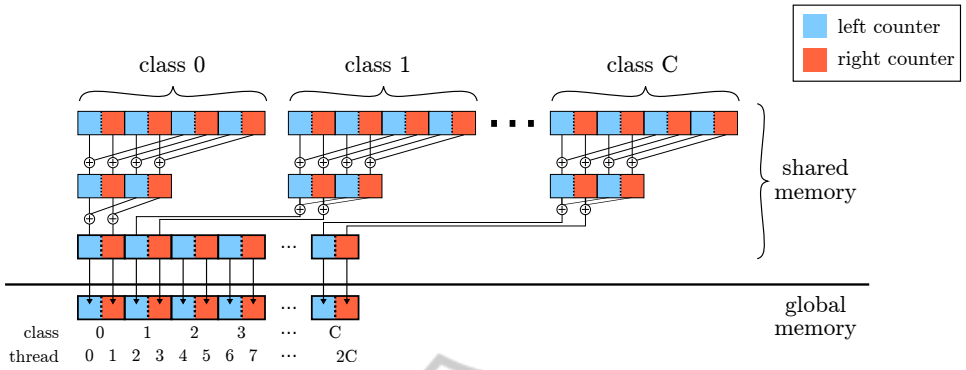

Figure 4: Reduction of histogram counters. Every thread sums to a dedicated left and right counter (indicated by different colors) for each class (first row). Counters are reduced in a subsequent phase. The last reduction step stores counters in shared memory, such that no bank conflicts occur when copying to global memory.

5.1 GPU Kernels

Random Feature and Threshold Candidate Generation. A significant amount of training time is used for generating random feature candidates. The total time for feature generation increases per tree level since the number of nodes increases as trees are grown.

The first step in the feature candidate generation is to randomly select feature parameter values. These are stored in a $F \times 11$ matrix for F feature candidates and eleven feature parameters of Eq. (1). The second step is the selection of one or more thresholds for every feature candidate. Random threshold candidates can either be obtained by randomly sampling from a distribution or by sampling feature responses of training instances. We implement the latter approach, which allows for greater flexibility if features or image channels are changed. For every feature candidate generation, one thread on the GPU is used and all T thresholds for a given feature are sampled by the same thread.

In addition to sorting samples according to the image they belong to, feature candidates are sorted by the feature type, channels used, and region offsets. Sorting reduces branch divergence and improves spatial locality, thereby increasing the cache hit rate.

Feature Response Calculation. The GPU implementation uses a similar optimization technique to the one used on the CPU, where loops in the feature generation step are rearranged in order to improve caching.

We used one thread to calculate the feature response for a given feature and a given training sample. Figure 3(a) shows the thread block layout for the feature response calculation. A row of blocks calculates all feature responses for a given sample. A column of blocks calculates the feature responses for a given feature over all samples. The dotted red arrow indicates the order of thread block scheduling. The execution order of thread blocks is determined by calculating the Block ID *bid*. In the two-dimensional case, it is defined as

$$bid = \text{blockIdx}.x + \underbrace{\text{gridDim}.x}_{\text{blocks in row}} \cdot \underbrace{\text{blockIdx}.y}_{\text{sample ID}}.$$

The number of features can exceed the maximum number of threads in a block, hence, the feature response calculation is split into several thread blocks. We use the x coordinate in the grid for the feature block to ensure that all features are evaluated before the GPU continues with the next sample. The y coordinate in the grid assigns training samples to thread blocks. Threads reconstruct their feature ID f using block size, thread and block ID by calculating

$$f = \text{threadIdx}.x + \underbrace{\text{blockDim}.x}_{\text{threads in block row}} \cdot \underbrace{\text{blockIdx}.x}_{\text{block index in grid row}}.$$

After sample data and feature parameters are loaded, the kernel calculates a single feature response for a depth or color feature by querying four pixels in an integral image and carrying out simple arithmetic operations to calculate the two regions sums and their difference.

Histogram Aggregation. Feature responses are aggregated into class histograms. Counters for histograms are maintained in a four-dimensional matrix of size $F \times T \times C \times 2$ for F features, T thresholds, C classes, and the two left and right children of a split.

To compute histograms, the iteration over features and thresholds is implemented as thread blocks in a two-dimensional grid on GPU; one thread block per feature and threshold. This is depicted in Fig. 3(b). Each thread block slices samples into partitions such that all threads in the block can aggregate histogram counters in parallel.

Histogram counters for one feature and threshold are kept in the shared memory, and every thread gets a distinct region in the memory. For X threads and C classes, $2XC$ counters are allocated. An additional reduction phase is then required to reduce the counters to a final sum matrix of size $C \times 2$ for every feature and threshold.

Figure 4 shows histogram aggregation and sum reduction. Every thread increments a dedicated counter for each class in the first phase. In the next phase, we iterate over all C classes and reduce the counters of every thread in $O(\log X)$ steps, where X is the number of threads in a block. In a single step, every thread calculates the sum of two counters. The loop over all classes can be executed in parallel by $2C$ threads that copy the left and right counters of C classes.

The binary reduction of counters (Fig. 4) has a constant runtime overhead per class. The reduction of counters for classes without samples can be skipped, as all counters are zero in this case.

Impurity Score Calculation. Computing impurity scores from the four-dimensional counter matrix is the last of the four training phases that are executed on GPU.

In the score kernel computation, 128 threads per block are used. A single thread computes the score for a different pair of features and thresholds. It loads $2C$ counters from the four-dimensional counter matrix in global memory, calculates the impurity score and writes back the resulting score to global memory.

The calculated scores are stored in a $T \times F$ matrix for T thresholds and F features. The matrix is then finally transferred from device to host memory space.

Undefined Values. Image borders and missing depth values (e.g. due to material properties or camera disparity) are represented as NaN, which automatically propagates and causes comparisons to produce *false*. This is advantageous, since no further checks are required and the random forest automatically learns to deal with missing values.

5.2 Global Memory Limitations

Slicing of Samples. Training arbitrarily large datasets with many samples can exceed the storage capacity of global memory. The feature response matrix of size $D \times F$ scales linearly in the number of samples D and the number of feature candidates F. We cannot keep the entire matrix in global memory if D or F is too large. For example, training a dataset with 500 images, 2000 samples per image, 2000 feature candidates and double precision feature responses (64 bit) would require $500 \cdot 2000 \cdot 2000 \cdot 64\,\text{bit} \approx 15\,\text{GB}$ of global memory for the feature response matrix in the root node split evaluation.

To overcome this limitation, we split samples into partitions, sequentially compute feature responses, and aggregate histograms for every partition. The maximum possible partition size depends on the available global memory of the GPU.

Image Cache. Given a large dataset, we might not be able to keep all images in the GPU global memory. We implement an image cache with a last recently used (LRU) strategy that keeps a fixed number of images in memory. Slicing samples ensures that a partition does not require more images than can be fit into the cache.

Memory Pooling. To avoid frequent memory allocations, we reuse memory that is already allocated but no longer in use. Due to the structure of random decision trees, evaluation of the root node split criterion is guaranteed to require the largest amount of memory, since child nodes always contain less or equal samples than the root node. Therefore, all data structures have at most the size of the structures used for calculating the root node split. With this knowledge, we are able to train a tree with no memory reallocation.

5.3 Extensions

Hyper-parameter Optimization. Cross-validating all the hyper-parameters is a requirement for model comparison, and random forests have quite a few hyper-parameters, such as stopping criteria for splitting, number of features and thresholds generated, and the feature distribution parameters.

To facilitate model comparison, CURFIL includes support for cross-validation and a client for an informed search of the best parameter setting using Hyperopt (Bergstra et al., 2011). This allows to leverage the improved training speed to run many experiments serially and in parallel.

Image Flipping. To avoid overfitting, the dataset can be augmented using transformations of the training dataset. One possibility is to add horizontally flipped images, since most tasks are invariant to this transformation. CURFIL supports training horizontally flipped images with reduced overhead.

Instead of augmenting the dataset with flipped images and doubling the number of pixels used for training, we horizontally flip each of the two rectangular regions used as features for a sampled pixel. This is equivalent to computing the feature response of the same feature for the same pixel on an actual flipped image. Histogram counters are then incremented following the binary test of both feature responses. The

Table 1: Comparison of random forest *training* time (in minutes) on a quadcore CPU and two non-mobile GPUs. Random forest parameters were chosen for best accuracy.

	NYU		MSRC	
Device	time	factor	time	factor
i7–4770K	369	1.0	93.2	1.0
Tesla K20c	55	6.7	5.1	18.4
GTX Titan	24	15.4	3.4	25.9

Table 2: Random forest *prediction* time in milliseconds, on RGB-D images at original resolution, comparing speed on a recent quadcore CPU and various GPUs. Random forest parameters are are chosen for best accuracy.

	NYU		MSRC-21	
Device	time	factor	time	factor
i7-440K	477	1	409	1
GTX 675M	28	17	37	11
Tesla K20c	14	34	10	41
GTX Titan	12	39	9	48

implicit assumption here is that the samples generated through flipping are independent.

The paired sample is propagated down a tree until the outcome of a node binary test is different for the two feature responses, indicating that a sample and its flipped counterpart should split into different directions. A copy of the sample is then created and added to the samples list of the other node child.

This technique reduces training time since choosing independent samples from actually flipped images requires loading more images in memory during the best split evaluation step. Since our performance is largely bounded by memory throughput, dependent sampling allows for higher throughput at no cost in accuracy.

6 EXPERIMENTAL RESULTS

We evaluate our library on two common image labeling tasks, the NYU Depth v2 dataset and the MSRC-21 dataset. We focus on the processing speed, but also discuss the prediction accuracies attained. Note that the speed between datasets is not comparable, since dataset sizes differ and the forest parameters were chosen separately for best accuracy.

The NYU Depth v2 dataset by (Silberman et al., 2012) contains 1,449 densely labeled pairs of aligned RGB-D images from 464 indoor scenes. We focus on the semantic classes *ground, furniture, structure*, and *props* defined by (Silberman et al., 2012).

Table 3: Segmentation accuracies on NYU Depth v2 dataset of our random forest compared to state-of-the-art methods. We used the same forest as in the training/prediction time comparisons of Tables 1 and 2.

	Accuracy [%]	
Method	Pixel	Class
(Silberman et al., 2012)	59.6	58.6
(Couprie et al., 2013)	63.5	64.5
Our random forest*	68.1	65.1
(Stückler et al., 2013)**	70.6	66.8
(Hermans et al., 2014)	68.1	69.0
(Müller and Behnke, 2014)**	72.3	71.9

* see main text for hyper-parameters used
** based on our random forest prediction.

To evaluate our performance without depth, we use the MSRC-21 dataset[3]. Here, we follow the literature in treating rarely occuring classes *horse* and *mountain* as *void* and train/predict the remaining 21 classes on the standard split of 335 training and 256 test images.

Tables 1 and 2 show random forest training and prediction times, respectively, on an Intel Core i7-4770K (3.9 GHz) quadcore CPU and various NVidia GPUs. Note that the CPU version is using all cores.

For the RGB-D dataset, training speed is improved from 369 min to 24 min, which amounts to a speed-up factor of 15. Dense prediction improves by factor of 39 from 477 ms to 12 ms.

Training on the RGB dataset is finished after 3.4 min on a GTX Titan, which is 26 times faster than CPU (93 min). For prediction, we achieve a speed-up of 48 on the same device (9 ms vs. 409 ms).

Prediction is fast enough to run in real time even on a mobile GPU (GTX 675M, on a laptop computer fitted with a quadcore i7-3610QM CPU), with 28 ms (RGB-D) and 37 ms (RGB).

Our implementation is fast enough to train hundreds of random decision trees per day on a single GPU. This fast training enabled us to conduct an extensive parameter search with cross-validation to optimize segmentation accuracy of a random forest trained on the NYU Depth v2 dataset (Silberman et al., 2012). Table 3 shows that we outperform other state-of-the art methods simply by using a random forest with optimized parameters. Our implementation was used in two publications which improved the results further by 3D accumulation of predictions in real time (Stückler et al., 2013) and superpixel CRFs (Müller and Behnke, 2014). This shows that efficient hyper-parameter search is crucial for model selection. Example segmentations are displayed in Figs. 5 and 6.

[3] http://jamie.shotton.org/work/data.html

Figure 5: Image labeling examples on NYU Depth v2 dataset. Left to right: RGB image, depth visualization, ground truth, random forest segmentation.

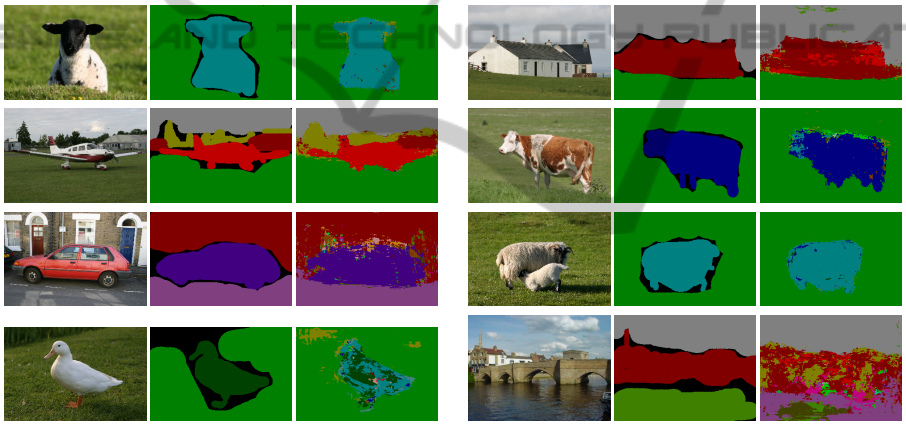

Figure 6: Image labeling examples on the MSRC-21 dataset. In groups of three: input image, ground truth, random forest segmentation. Last row shows typical failure cases.

Methods on the established RGB-only MSRC-21 benchmark are so advanced that their accuracy cannot simply be improved by a random forest with better hyper parameters. Our pixel and class accuracies for MSRC-21 are 59.2 % and 47.0 %, respectively. This is still higher than other published work using random forests as the baseline method, such as 49.7 % and 34.5 % by (Shotton et al., 2008). However, as (Shotton et al., 2008) and the above works show, random forest predictions are fast and constitute a good initialization for other methods such as conditional random fields.

Finally, we trained the MSRC-21 dataset by augmenting the dataset with horizontally flipped images using the naïve approch and our proposed method. The naïve approach doubles both the total number of samples and the number of images, which quadruples the training time to 14.4 min. Accuracy increases to 60.6 % and 48.6 % for pixel and class accuracy, respectively. With paired samples (introduced in Section 5.3), we reduce the runtime by a factor of two (to now 7.48 min) at no cost in accuracy (60.9 % and 49.0 %). The remaining difference in speed is mainly explained by the increased number of samples, thus the training on flipped images has very little overhead.

Random Forest Parameters. The hyper-parameter configurations for which we report our timing and accuracy results were found with cross-validation. The cross-validation outcome varies between datasets.

For the NYU Depth v2 dataset, we used three trees with 4537 samples / image, 5729 feature candidates / node, 20 threshold candidates, a box radius of

111 px, a region size of 3, tree depth 18 levels, and minimum samples in leaf nodes 204.

For MSRC-21 we found 10 trees, 4527 samples / image, 500 feature candidates / node, 20 threshold candidates, a box radius of 95 px, a region size of 12, tree depth 25 levels, and minimum samples in leaf nodes 38 to yield best results.

7 CONCLUSION

We provide an accelerated random forest implementation for image labeling research and applications. Our implementation achieves dense pixel-wise classification of VGA images in real-time on a GPU. Training is accelerated on GPU by a factor of up to 26 compared to an optimized CPU version. The experimental results show that our fast implementation enables effective parameter searches that find solutions which outperform state-of-the art methods. CURFIL prepares the ground for scientific progress with random forests, e.g. through research on improved visual features.

REFERENCES

Amit, Y. and Geman, D. (1997). Shape quantization and recognition with randomized trees. *Neural computation*, 9(7):1545–1588.

Bergstra, J., Bardenet, R., Bengio, Y., Kégl, B., et al. (2011). Algorithms for hyper-parameter optimization. In *Neural Information Processing Systems (NIPS)*.

Breiman, L. (2001). Random forests. *Machine learning*, 45(1):5–32.

Couprie, C., Farabet, C., Najman, L., and LeCun, Y. (2013). Indoor semantic segmentation using depth information. *The Computing Resource Repository (CoRR) abs/1301.3572*.

Hermans, A., Floros, G., and Leibe, B. (2014). Dense 3d semantic mapping of indoor scenes from rgb-d images. In *Int. Conf. on Robotics and Automation (ICRA)*, Hong Kong. IEEE.

Ho, T. (1995). Random decision forests. In *Int. Conf. on Document Analysis and Recognition (ICDAR)*, volume 1, pages 278–282. IEEE.

Lepetit, V. and Fua, P. (2006). Keypoint recognition using randomized trees. *Pattern Analysis and Machine Intelligence, IEEE Transactions on*, 28(9):1465–1479.

Lepetit, V., Lagger, P., and Fua, P. (2005). Randomized trees for real-time keypoint recognition. In *Computer Vision and Pattern Recognition (CVPR), Conf. on*, volume 2, pages 775–781.

Liao, Y., Rubinsteyn, A., Power, R., and Li, J. (2013). Learning random forests on the gpu. In *NIPS Workshop on Big Learning: Advances in Algorithms and Data Management*.

Müller, A. C. and Behnke, S. (2014). Learning depth-sensitive conditional random fields for semantic segmentation of rgb-d images. In *Int. Conf. on Robotics and Automation (ICRA)*, Hong Kong. IEEE.

Rodrigues, J., Kim, J., Furukawa, M., Xavier, J., Aguiar, P., and Kanade, T. (2012). 6D pose estimation of textureless shiny objects using random ferns for bin-picking. In *Intelligent Robots and Systems (IROS), Int. Conf. on*, pages 3334–3341. IEEE.

Sharp, T. (2008). Implementing decision trees and forests on a GPU. In *Europ. Conf. on Computer Vision (ECCV)*, pages 595–608.

Shotton, J., Fitzgibbon, A., Cook, M., Sharp, T., Finocchio, M., Moore, R., Kipman, A., and Blake, A. (2011). Real-time human pose recognition in parts from single depth images. In *Computer Vision and Pattern Recognition (CVPR), Conf. on*, pages 1297–1304.

Shotton, J., Johnson, M., and Cipolla, R. (2008). Semantic texton forests for image categorization and segmentation. In *Computer Vision and Pattern Recognition (CVPR), Conf. on*.

Silberman, N., Hoiem, D., Kohli, P., and Fergus, R. (2012). Indoor segmentation and support inference from RGBD images. In *Europ. Conf. on Computer Vision (ECCV)*, pages 746–760.

Slat, D. and Lapajne, M. (2010). *Random Forests for CUDA GPUs*. PhD thesis, Blekinge Institute of Technology.

Stückler, J., Biresev, N., and Behnke, S. (2012). Semantic mapping using object-class segmentation of RGB-D images. In *Intelligent Robots and Systems (IROS), Int. Conf. on*, pages 3005–3010. IEEE.

Stückler, J., Waldvogel, B., Schulz, H., and Behnke, S. (2013). Dense real-time mapping of object-class semantics from RGB-D video. *Journal of Real-Time Image Processing*.

Van Essen, B., Macaraeg, C., Gokhale, M., and Prenger, R. (2012). Accelerating a random forest classifier: Multi-core, GP-GPU, or FPGA? In *Int. Symp. on Field-Programmable Custom Computing Machines (FCCM)*. IEEE.

Viola, P. and Jones, M. (2001). Rapid object detection using a boosted cascade of simple features. In *Computer Vision and Pattern Recognition (CVPR), Conf. on*.

Wehenkel, L. and Pavella, M. (1991). Decision trees and transient stability of electric power systems. *Automatica*, 27(1):115–134.